Computer Aided Surgery 5:98–107 (2000)

Biomedical Paper

Comparative Tracking Error Analysis of Five Different Optical Tracking Systems

Rasool Khadem, Ph.D., Clement C. Yeh, M.S., Mohammad Sadeghi-Tehrani, M.S., Michael R. Bax, M.S., Jeremy A. Johnson, M.S., Jacqueline Nerney Welch, M.S., Eric P. Wilkinson, B.S.E., and Ramin Shahidi, Ph.D.
Image Guidance Laboratories, Stanford University School of Medicine, Stanford, California

ABSTRACT Objective: Effective utilization of an optical tracking system for image-based surgical guidance requires optimal placement of the dynamic reference frame (DRF) with respect to the tracking camera. Unlike other studies that measure the overall accuracy of a particular navigation system, this study investigates the precision of one component of the navigation system: the optical tracking system (OTS). The precision of OTS measurements is quantified as *jitter*. By measuring jitter, one can better understand how system inaccuracies depend on the position of the DRF with respect to the camera.

Materials and Methods: Both FlashPoint™ (Image Guided Technologies, Inc., Boulder, Colorado) and Polaris™ (Northern Digital Inc., Ontario, Canada) optical tracking systems were tested in five different camera and DRF configurations. A linear testing apparatus with a software interface was designed to facilitate data collection. Jitter measurements were collected over a single quadrant within the camera viewing volume, as symmetry was assumed about the horizontal and vertical axes.

Results: Excluding the highest 5% of jitter, the FlashPoint cameras had an RMS jitter range of 0.028 ± 0.012 mm for the 300 mm model, 0.051 ± 0.038 mm for the 580 mm model, and 0.059 ± 0.047 mm for the 1 m model. The Polaris camera had an RMS jitter range of 0.058 ± 0.037 mm with an active DRF and 0.115 ± 0.075 mm with a passive DRF.

Conclusion: Both FlashPoint and Polaris have jitter less than 0.11 mm, although the error distributions differ significantly. Total jitter for all systems is dominated by the component measured in the axis directed away from the camera. Comp Aid Surg 5:98–107 (2000). ©2000 Wiley-Liss, Inc.

Key words: **optical tracking system, tracking accuracy, image-guided surgery, stereotactic surgery**

INTRODUCTION

The rapid development of image-guided surgery has been made possible by recent advances in computer and optical hardware. These advances have streamlined the progression of image-guided systems from earlier, more primitive models. Conventional stereotactic systems, which require a rigid frame of reference to be bolted to the skull for patient-image registration, are being replaced by frameless systems that define the reference space using small, removable fiducial markers or other equivalent devices. These devices have increased the surgeon's flex-

Address correspondence/reprint requests to: Ramin Shahidi, Image Guidance Laboratories, Department of Neurosurgery, 300 Pasteur Dr., MC: 5327, Stanford CA, 94305-5327; Telephone: (650) 498-7958; Fax: (650) 724-4846; E-mail: shahidi@stanford.edu.

©2000 Wiley-Liss, Inc.

ibility and freedom during surgery. The advances in image-guided surgery have been implemented for intraoperative navigational assistance for management of orthopedic,[9,10,18,25,33] neurosurgical,[1,5,20,26,31] craniofacial, otolaryngologic[16] and general surgical problems. Since the advent of the stereotactic frame, a number of systems have been developed that register patient images to the reference space and then track the patient post-registration.[29] These systems include mechanical stereotactic articulated arms,[3,13,36] vision-based optical tracking systems,[12,17,34] acoustical systems,[11,32,35] and magnetic systems.[2,4,8,22,27,28]

The creation of newer navigation systems has raised questions about the accuracy of the systems themselves. Freedom of movement without the constraints of conventional stereotactic hardware has increased the propensity for errors. Recent studies on the overall accuracy of image-guided systems have reported errors of 2-3 mm.[7,23,37] Caversaccio et al. have reported sub-millimeter accuracy,[6] although these results have not been widely reproduced.

Several recent studies have addressed the accuracy of image-guided tracking systems and their components. The accuracy of magnetic tracking systems has been studied for use in kinesiologic studies,[2,27] catheter-based applications,[22] and recently with new long-range transmitters.[8,27] Optical tracking system accuracy has been studied in the context of tracking a surgical tool with respect to the patient, as discussed above, but has also been studied when the LEDs are attached to a microscope and used to track the focal point of the microscope with respect to patient data.[14,16,21,23,24] Hybrid magnetic-optical systems are beginning to be tested; a recent study showed less than 2 mm of positional error when using such a system in combination with distortion reduction routines.[4] Wireless optical marker systems have also been introduced as an alternative to conventional wired systems.[30]

Sasama[33] assessed the accuracy of the Optotrak™ (Northern Digital Inc., Ontario, Canada) optical tracking system in the setting of orthopedic total hip arthroplasty. His group used the iterative closest-point algorithm to assess tool tracking, and had results of less than 1 mm of positional error and less than a degree of rotational error. Rohling et al.[31] compared the accuracy of the Optotrak optical tracking system to the FARO mechanical arm (Faro Technologies, Lake Mary, Florida) using a milled metal block as a standard. They found that Optotrak's accuracy is within the manufacturer's specifications of 0.15 mm with a distance of 2.5 m between the CCD cameras and the LEDs. The FARO mechanical arm is less accurate, but sufficient for use in surgical image guidance. Ryan[32] describes the implementation of a frameless stereotactic system using a dynamic reference frame, but utilizes 150 points on the patient's head and a surface-matching algorithm instead of externally placed fiducial markers for patient registration. The calculated distance between the location of the target point and the stereotactically selected point was designated as the system accuracy and was reported to be 4.8 ± 3.5 mm. Chassat and Lavallée[7] describe optical tracking system accuracy tests by comparing four different CCD-based systems using four tests: an intrinsic accuracy test, a rigid deformation test, a pivot test, and a surface digitization test.

Optical tracking system (OTS) accuracy investigations are also being performed to assess the viability of OTS application for surgical robotic and radiotherapeutic applications. Hassfeld et al.[15] report 2–3 mm of accuracy on their image-guidance system using the Polaris OTS, and have begun to incorporate a control system for their PUMA 260 robotic arm using the tracking system. Kai et al.[19] implemented a system to use the Optotrak OTS to track head motion in frameless stereotactic radiosurgery and assessed the standard deviation measurements of the system.

The study described in this paper is the first of a series aimed at characterizing optical tracking systems. Unlike other studies that focus on the behavior of a complete surgical navigation system, this study and those to follow will investigate the properties of a single component of a navigation system: the optical tracking system. By taking the results of this study into account when designing a navigation system, the OTS measurements will be more precise, improving overall system performance.

The OTS is responsible for reporting the location and orientation of a dynamic reference frame (DRF) and a tool to be tracked. Figure 1 shows the DRFs used in this experiment. These tracking systems consist of two or more detectors (one- or two-dimensional image sensors) and emitters (infrared light-emitting diodes (LEDs)). In the *active* configuration, the emitters are mounted on the DRF. The OTS compares the location of the LEDs in images obtained from sensors located in the camera and determines the location and orientation of the DRF relative to the camera using a triangulation technique. In the *passive* configuration, the infrared light is emitted from the camera unit and

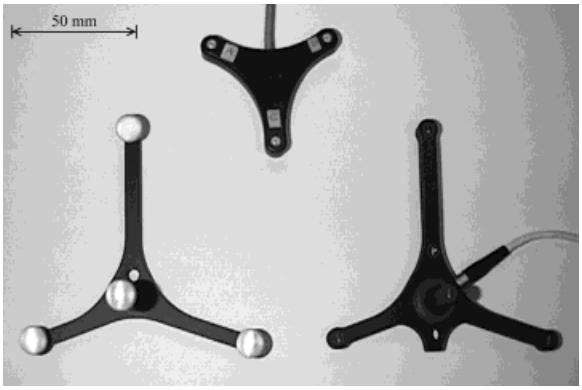

Fig. 1. Dynamic Reference Frames (DRFs). Testing was done using a three-LED DRF for the FlashPoint cameras (top), a four-reflector DRF for the passive NDI camera (left), and a four-LED DRF for the active NDI camera (right).

reflected from spheres mounted on the DRF. The OTS uses the light reflected from the spheres rather than light transmitted from LEDs on the DRF to determine the location and orientation of the DRF.

Ideally, the OTS would report the true location and orientation of the DRF and would be constant for multiple readings of a stationary DRF. However, errors do arise in OTS measurements for several reasons, including quantization due to a finite number of pixels in the image sensor, imperfect optics, and inaccuracies due to triangulating the position of each emitter. If the average of multiple readings does not converge to the correct location and orientation, the system is biased; if multiple readings are not closely grouped, the system is imprecise. This study measures the precision of OTS position measurements. Since precision is a qualitative term, *jitter* is used to quantify the deviation of repeated measurements from the mean. Jitter is defined to be the standard deviation of a series of OTS measurements of a stationary DRF about their sample mean.

Jitter measurements were obtained at positions uniformly spaced throughout a three-dimensional volume for each OTS. Through an analysis of the jitter, the influence of the DRF location on the precision of OTS position measurements can be better understood.

METHODS

The volume measurements were obtained through the use of a precision-machined linear testing apparatus (LTA), shown in Figure 2. The primary component of the LTA consists of a 500 mm^2 target mounting plate with a 10×10 grid of uniformly spaced holes. The holes are separated by 50 mm in both directions at 0.003 mm tolerance. A mount with pegs that mate with the holes in the target mounting plate is used to attach the DRF to the grid. The position of the DRF can therefore be easily varied in two dimensions. In order to obtain measurements in the third dimension, the plate is placed on a linear track. A threaded shaft runs along the linear track and allows movement in the direction normal to the plane within a range of 700 mm.

An optical tracking system is a unique combination of camera and DRF. Table 1 lists the five system configurations tested in this experiment. When testing the Image Guided Technologies (IGT) FlashPoint camera, an IGT 50 mm DRF with three infrared LEDs was utilized. For the tests of the Northern Digital Inc. (NDI) passive Polaris system, a TA002 DRF (Traxtal Technologies, Bellaire, TX) with four reflecting balls was employed. With the NDI active Polaris configuration, an active DRF identical to the TA002 model in size and shape, but with four active infrared LEDs, was used. For the NDI tracking units, the viewing angle is a parameter which can be set by the user. If the system is operated inside the viewing angle, the magnitude of error should not exceed the manufacturer's performance claim. Since the viewing angle varies inversely with the accuracy reported by the manufacturer, the smallest possible angle (30 de-

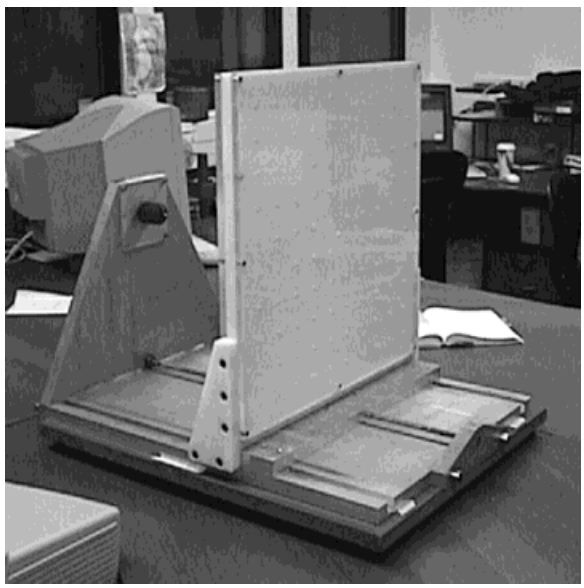

Fig. 2. Linear testing apparatus.

Table 1. Optical Tracking System Configurations Tested. Tests were performed for a wide range of camera sizes, as indicated in the last column.

System	DRF used	Distance between outermost image sensors [mm]
IGT 300 mm FlashPoint	3 LED 50 mm active IGT	200
IGT 580 mm FlashPoint	3 LED 50 mm active IGT	480
IGT 1 m FlashPoint	3 LED 50 mm active IGT	1000
NDI Polaris	4 LED Active TRAXTAL	480
NDI Polaris (passive)	4 LED Passive TRAXTAL	480

grees) was chosen to maximize the precision of this system.

There is a range of positions inside of which the tracking apparatus is completely visible to the camera and for which valid measurements can be made. This region is called the digitizing volume and varies significantly between cameras. The volume over which measurements were taken encompassed much of the digitizing volumes of the cameras and was large enough to include the working field for a surgical application. The digitizing and measurement volume dimensions are specified in Table 2.

For any fixed position between the LTA and the camera, there is a 700 mm $\times$ 450 mm $\times$ 450 mm volume (LTA volume unit) where measurements can be taken. In order to achieve the entire measurement volume for a single camera and tracking apparatus, the relative position must be varied in all three dimensions and the LTA volume units combined to compose the full data set. It is assumed that the digitizing volume is symmetric about the *x* and *y* axes, therefore measurements only need to be recorded in a single quadrant. Figure 3 illustrates the position of the camera relative to the LTA, as well as the digitizing and tested volumes.

The LTA volume was moved left, right, towards, and away from the camera in order to build the measurement volume in two of the dimensions. The third dimension of the measurement volume was sampled by changing the height of the camera on the tripod. Each time the LTA or camera was repositioned, an alignment procedure was necessary to maintain the parallel configuration of the sampling intervals.

The LTA was placed on a table in front of the camera with its plane parallel to the *x*-*y* plane of the camera. First, the tracking apparatus was mounted in the top left position on the LTA plate. The camera mounted on a tripod was repositioned until the values read from the camera were at the origin of the *x*-*y* plane. The tracking apparatus was then positioned serially in the four corners of the plate to verify that the plane of the plate was parallel to the camera. One hundred data points were collected from the first position. Next, the tracking apparatus was moved 10 cm to the right for the collection of another 100 data points. This was repeated for 5 positions on each of 5 rows, for a total of 25 positions. Subsequently, the plate was shifted a distance of 10 cm along the *z*-axis — away from the camera — using a threaded shaft. This entire process would be repeated at 10-cm intervals along the length of the linear track. Once one LTA volume unit had been sampled, either the LTA or camera would be repositioned to attain the next portion of the measurement volume.

Table 2. Dimensions of the Vendor-Specified Digitizing Volume and of the Tested Volume. The digitizing volume consists of the region within which the OTS can report accurate values. The tested volume is a similar region that overlaps with the digitizing volume and over which measurements were made for this study.

Camera	Max *X* spec [mm]	Max *X* tested [mm]	Max *Y* spec [mm]	Max *Y* tested [mm]	Min *Z* spec [mm]	Min *Z* tested [mm]	Max *Z* spec [mm]	Max *Z* tested [mm]
300 mm Flashpoint	150	300	150	400	600	600	900	900
580 mm Flashpoint	500	430	500	650	1000	1060	2000	2160
1 m Flashpoint	500	800	500	650	1000	1060	2000	2160
Polaris	500	410	500	620	1400	1400	2400	2400
Polaris (passive)	500	350	500	620	1400	1400	2400	2400

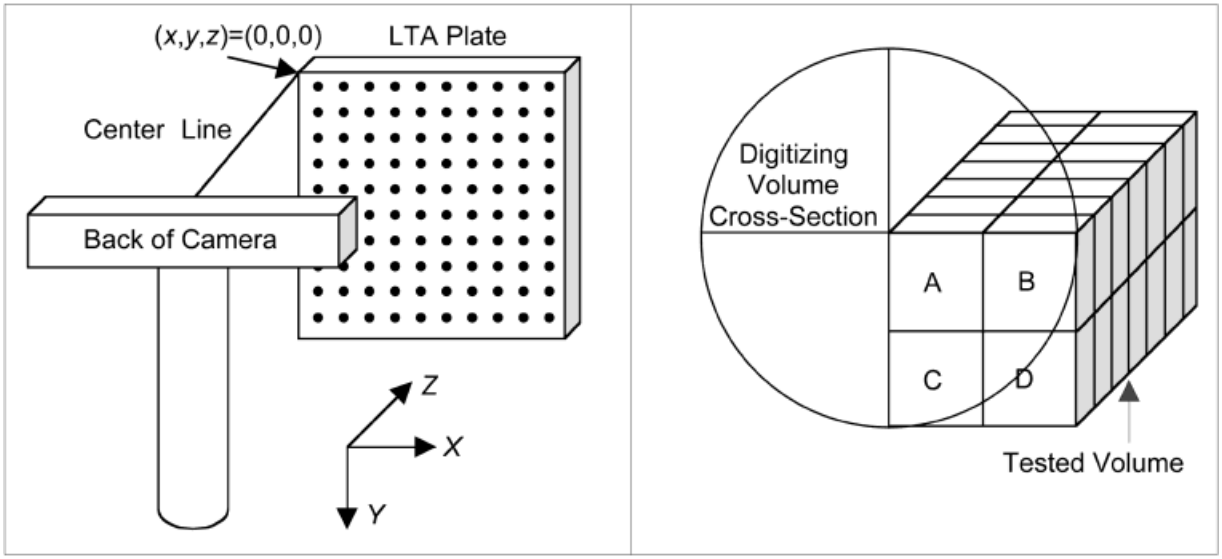

Fig. 3. Left: The relative position of the camera, the LTA plate, and the *X*, *Y*, and *Z* axes. Right: The actual digitizing volume reconstruction. The reported results for A, B, C, and D were used to reconstruct the other quadrant values based on symmetry.

The spatial *x*, *y*, and *z* coordinates were consecutively sampled 100 times at each sensor position to give (X_i, Y_i, Z_i), for $1 \leq i \leq 100$. Four jitter measurements were calculated relative to the mean coordinates (μ_X, μ_Y, μ_Z) at each position: the jitter J is the standard deviation of the Euclidean distances

$$\left\| [X_i \; Y_i \; Z_i]^T - [\mu_X \; \mu_Y \; \mu_Z]^T \right\| \tag{1}$$

normalized for the sample population; its components J_X, J_Y, and J_Z are the normalized standard deviation of each of the *x*, *y*, and *z* coordinates. These are estimates of the total jitter and its components along each axis for a given sensor location.

RESULTS

A review of the raw data revealed that a small subset of the sample data appeared to be affected by time-varying external disturbances to the camera or LTA. Typical disturbances consisted of a constant velocity or oscillation predominantly in the *x*-axis direction, resulting in highly correlated sample sequences. Since the purpose of this study was to examine jitter under undisturbed (static) conditions, these sequences were removed from the dataset.

Figure 4 shows the mean jitter as a function of distance from each camera along the *z*-axis. The mean of the lowest 95% of the jitter values in each constant-*z* set was computed and plotted against *z*. These points were used to find a least-squares fit for a quadratic model of mean jitter as a function of z_m (*z* measured in meters):

$$J(z) \approx \frac{az_m^2 + bz_m + c}{10000} \tag{2}$$

The figure shows the coefficients *a*, *b*, and *c* for each camera. Also shown are the ranges in *z* for which each camera's jitter was calculated.

Figure 5 shows the relative magnitudes of the jitter components and how they vary within the reported volume. The legend indicates the meaning of the dimensions of the ellipse pairs; the details follow below.

Each pair of concentric ellipses in a given plane represents the extremes of the separate components of jitter in that plane for the set of all sensor positions that share the coordinates of that ellipse pair's center. The set may be visualized as the set of all sensor positions along a line which is perpendicular to the plane of the ellipses and intersects that plane at the center of the ellipse pair.

The distance along the vertical axis of an ellipse, from its center to its boundary, shows the jitter component along the vertical axis of the graph. Likewise, the horizontal distance shows the jitter component along the horizontal axis. The outer ellipse shows the maximum of the individual jitter components' magnitudes, and the inner ellipse

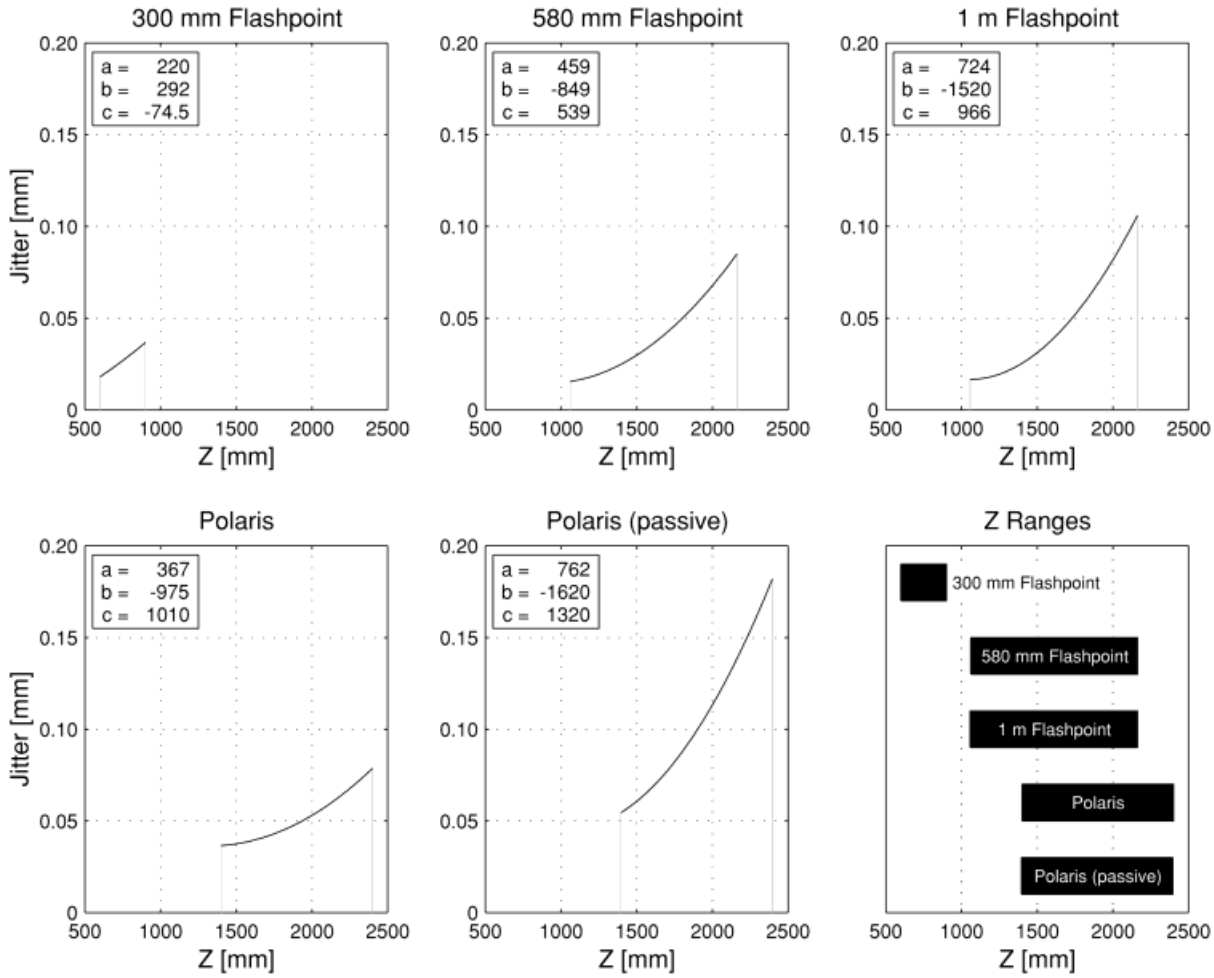

Fig. 4. Jitter as a function of depth.

shows the magnitudes of the minimum individual jitter components at the set of positions defined above. The extremes of the jitter components along separate axes are selected independently and do not *necessarily* correspond to common sensor positions. The ellipses have been scaled up by a factor of 400. The full curve of the ellipse is shown to facilitate an interpretation of the relative magnitudes of the jitter along each axis; the curve itself gives no information other than the lengths of its axes.

Figure 6 shows the worst-case, or maximum, jitter values of each camera: first considering all the jitter values, and second considering only the lowest 95% of the jitter values. The lowest 95% of jitter values exhibit an RMS jitter range of 0.028 $\pm$ 0.012 mm for the FlashPoint 300 mm camera, 0.051 $\pm$ 0.038 mm for the 580 mm model, and 0.059 $\pm$ 0.047 mm for the 1 m model. The Polaris camera had an RMS jitter range of 0.058 $\pm$ 0.037 mm with an active DRF and 0.115 $\pm$ 0.075 mm with a passive DRF. Table 3 details these results.

DISCUSSION

The data show that jitter is dominated by jitter in the *z* direction, which increases with increasing *z*. This confirms the hypothesis that the best method to improve OTS precision is to decrease the distance between the target and tracking apparatus. The *x* and *y* jitter components are insignificant compared to the *z* component, and are roughly equal in magnitude.

These findings can be used to design an OTS and working field configuration that optimizes precision. First, the OTS camera should be as close as possible to the surgical field. Other requirements limit how close the camera can be to the surgical field, such as the need to work between the two,

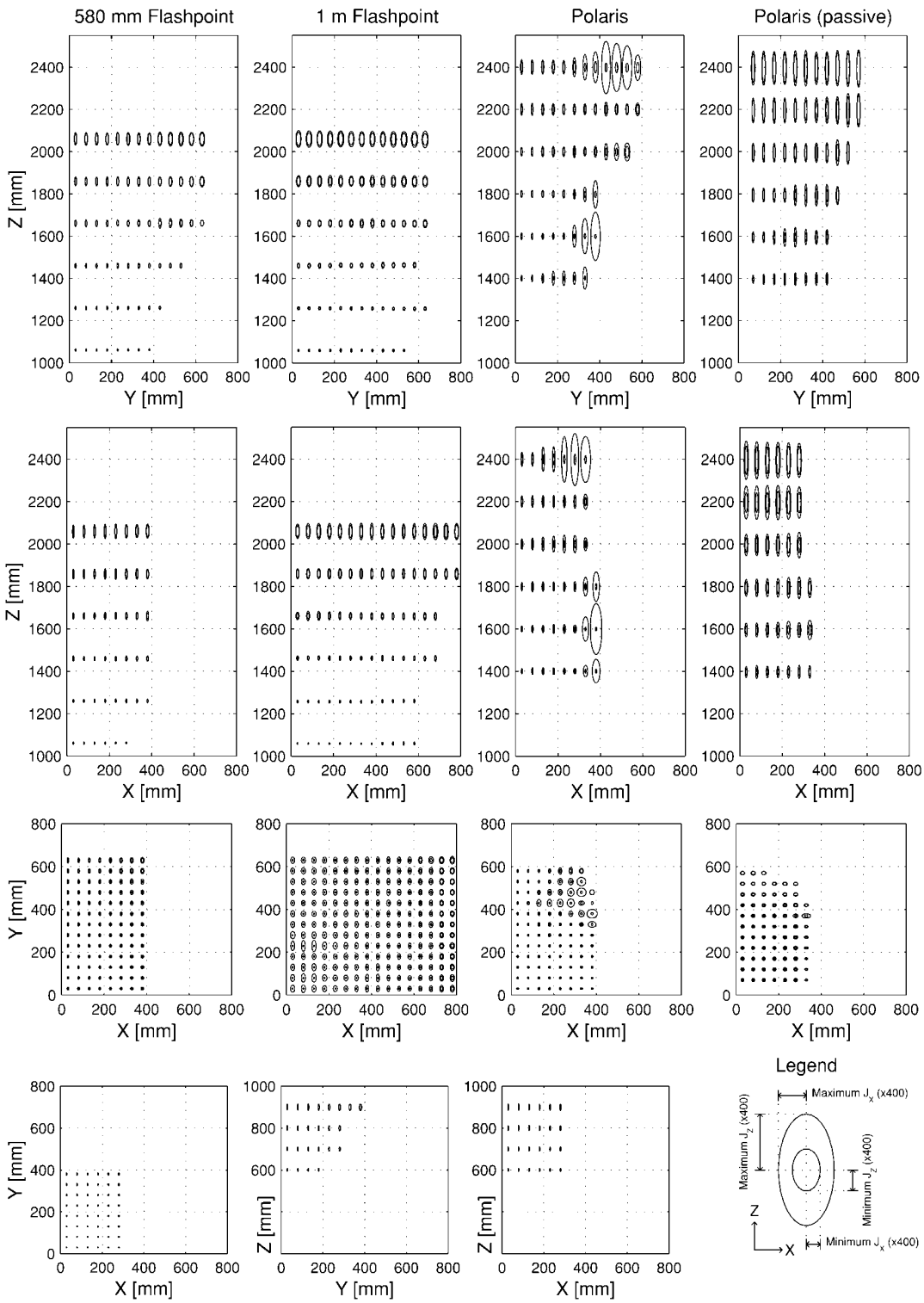

Fig. 5. Three-dimensional distribution of jitter values.

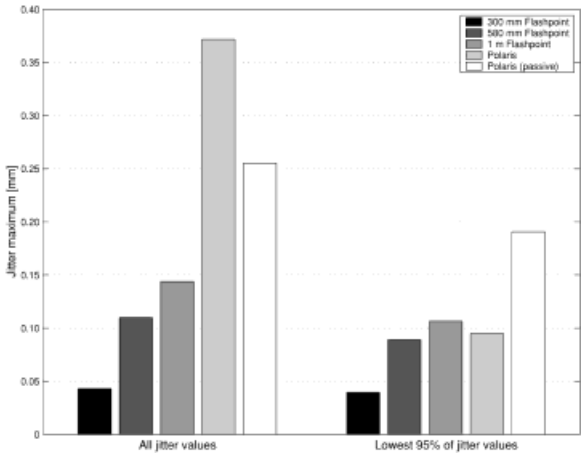

Fig. 6. Camera maximum jitter values.

and the need for a digitizing volume large enough to encompass the field. Second, the orientation of the camera should be such that the direction that is least clinically significant — the direction in which the most imprecision can be tolerated — is aligned with the camera *z*-axis. Once this constraint has been met, the camera can be rotated to any orientation around the *z*-axis without any sacrifice in precision.

The data also show that the active NDI Polaris camera has a much higher maximum jitter than the passive configuration or any of the IGT FlashPoint cameras. However, if outliers are excluded, the 580 mm FlashPoint camera and the NDI active systems are comparable, and both are more accurate than 300 mm FlashPoint or Polaris passive configurations. In testing, the IGT active systems were more predictable in their jitter error than the NDI active configuration. Applying a moving average filter on the data can increase the predictability in the reported reading at the expense of inherent lag. This delay, for instance, is equivalent to half of the averaging window length for a constant window, but can be shorter for other window designs. Further investigations on the effects of these findings on specific applications and ways to reduce them are planned.

The method presented for jitter measurement and analysis is independent of the tracking technology, and can be used for investigating the precision of future tracking systems. Precision of position readings, however, is only one consideration in selecting an optical tracking system. In surgical navigation applications, coordinates need to be continuously sampled for moving objects. The errors associated with this kind of utilization are more complicated than the error associated with static measurements. While jitter and other static errors give an estimate of the camera's inherent inaccuracies, it is expected that true overall error in tracking dynamic targets depends on more complex parameters that will be addressed in future work.

This study considered DRF positions that were parallel to the camera *x-y* plane, which does not accurately reflect the typical use of a tracking system. In clinical use of an OTS, the DRF can be in any orientation as long as all the LEDs or reflecting spheres are visible to the camera. A study of how the OTS precision varies with DRF orientation is underway.

The precision of position measurements made by five commercially available optical tracking systems has been quantified throughout a volume. For every OTS, the jitter component in the direction away from the face of the camera dominates the total jitter for any DRF position in the volume. Both the IGT and NDI systems have been shown to have roughly equivalent jitter magnitudes for cameras of the same length.

ACKNOWLEDGMENTS

We would like to thank Image Guided Technologies and Northern Digital Inc. for providing the optical tracking systems. We are also grateful to the following Stanford University faculty: Tom Krummel, M.D. for laboratory space, David P. Martin, M.D. for technical assistance with the navigation

Table 3. Camera Jitter Value Ranges

Camera	μ_j [mm]	Δ^+ [mm]	Δ^- [mm]	J_{center} [mm]	Δ [mm]
300 mm Flashpoint	0.028	0.012	−0.012	0.028	0.012
580 mm Flashpoint	0.046	0.044	−0.033	0.051	0.038
1 m Flashpoint	0.047	0.059	−0.035	0.059	0.047
Polaris	0.053	0.042	−0.032	0.058	0.037
Polaris (passive)	0.109	0.082	−0.068	0.115	0.075

hardware, and Gary K. Steinberg, M.D., Ph.D. and John R. Adler Jr., M.D. for making this work possible.

REFERENCES

1. Adler JR Jr. Indications and limitations of stereotactic radiosurgery. West J Med 1993;158:66.
2. An KN, Jacobsen MC, Berglund LJ, Chao EYS. Application of a magnetic tracking device to kinesiologic studies. J Biomech 1988;21:613–620.
3. Barnett GH, Steiner CP, Roberts DW. Surgical navigation system technologies. In: Barnett GH, Roberts DW, Maciunas RJ, editors: Image Guided Neurosurgery: Clinical Applications of Surgical Navigation. St. Louis: Quality Medical Publishing; 1998.
4. Birkfellner W, Watzinger F, Wanschitz F, Enislidis G, Truppe M, Ewers R, Bergmann H. Concepts and results in the development of a hybrid tracking system for CAS. In: Wells WM, Colchester A, Delp S, editors: Proceedings of First International Conference on Medical Image Computing and Computer Assisted Interventions (MICCAI'98), Cambridge, MA, October 1998. Lecture Notes in Computer Science 1496. Berlin, Heidelberg, New York: Springer-Verlag; 1998. p 343–351.
5. Bucholz RD, Ho HW, Rubin JP. Variables affecting the accuracy of stereotactic localization using computerized tomography. J Neurosurg 1993;79:667–673.
6. Caversaccio M, Ladrach K, Bachler R, Schroth G, Nolte LP, Hausler R. Computer-assisted surgical navigation with a dynamic mobile framework for the nasal fossae, sinuses and base of the skull (in French). Ann Otolaryngol Chir Cervicofac 1998;115:253–258.
7. Chassat F, Lavallée S. Experimental protocol of accuracy evaluation of 6-D localizers for computer-integrated surgery: Application to four optical localizers. In: Wells WM, Colchester A, Delp S, editors: Proceedings of First International Conference on Medical Image Computing and Computer Assisted Interventions (MICCAI'98), Cambridge, MA, October 1998. Lecture Notes in Computer Science 1496. Berlin, Heidelberg, New York: Springer-Verlag; 1998. p 277–284.
8. Day JS, Dumas GA, Murdoch DJ. Evaluation of a long-range transmitter for use with a magnetic tracking device in motion analysis. J Biomech 1998;31: 957–961.
9. Delp SL, Stulberg SD, Davies B, Picard F, Leitner F. Computer assisted knee replacement. Clinical Orthopaedics 1998;354:49–56.
10. DiGioia AM, Jamaraz B, O'Toole RV, Simon D, Kanade T. Medical robotics and computer assisted surgery in orthopaedics. In: Morgan K, Satava RM, Sieberg HB, Mattheus R, Christensen JP, editors: Interactive Technology and the New Paradigm for Healthcare. Burke, VA: IOS Press; 1994. p 88–90.
11. Friets EM, Strohbehn JW, Hatch JF, Roberts DW. A frameless stereotaxic operating microscope for neurosurgery. IEEE Trans Biomed Eng 1989;36:608–617.
12. Grimson E, Leventon M, Ettinger G, Chabrerie A, Ozlen F, Nakajima S, Atsumi H, Kikinis R, Black P. Clinical experience with a high precision image-guided neurosurgery system. In: Wells WM, Colchester A, Delp S, editors: Proceedings of First International Conference on Medical Image Computing and Computer Assisted Interventions (MICCAI'98), Cambridge, MA, October 1998. Lecture Notes in Computer Science 1496. Berlin, Heidelberg, New York: Springer-Verlag; 1998. p 63–73.
13. Guthrie BL, Adler JR Jr. Computer-assisted preoperative planning, interactive surgery, and frameless stereotaxy. Clin Neurosurg 1992;38:112–131.
14. Haller JW, Smith K, Ryken T, Caplan J, Vannier MW. Validation of an image-guided surgical navigation system. In: Lemke HU, Vannier MW, Inamura K, Farman AG, editors: Computer Aided Radiology and Surgery: Proceedings of the 13th International Congress and Exhibition (CARS'99), Paris, June 1999. Amsterdam: Elsevier; 1999. p 711–714.
15. Hassfeld S, Burghart C, Bertovic I, Raczkowsky J, Rembold U, Wörn H, Mühling J. Intraoperative navigation techniques: Accuracy tests and clinical report. In: Lemke HU, Vannier MW, Inamura K, Farman AG, editors: Computer Aided Radiology and Surgery: Proceedings of the 12th International Symposium and Exhibition (CAR'98), Tokyo, June 1998. Amsterdam: Elsevier; 1998. p 670–675.
16. Hauser R, Westermann B. Optical tracking of a microscope for image-guided intranasal sinus surgery. Ann Otol Rhinol Laryngol 1999;108:54–62.
17. Heilbrun MP, McDonald P, Wiker C, Koehler S, Peters W. Stereotactic localization and guidance using a machine vision technique. Stereotact Functional Neurosurg 1992;58:94–98.
18. Hsu HC, Luo ZP, Rand JA, An KN. Influence of patellar thickness on patellar tracking and patellofemoral contact characteristics after total knee arthroplasty. J Arthroplasty 1996;11:69–80.
19. Kai J, Shiomi H, Sasama T, Sato Y, Inoue T, Tamura S. An optical high-precision 3D position measurement system suitable for head motion tracking in frameless stereotactic radiosurgery. In: Lemke HU, Vannier MW, Inamura K, Farman AG, editors: Computer Aided Radiology and Surgery: Proceedings of the 12th International Symposium and Exhibition (CAR'98), Tokyo, June 1998. Amsterdam: Elsevier; 1998. p 599–604.
20. Kato A, Yoshimine T, Hayakawa T, Tomita Y, Ikeda T, Mitomo M, Harada K, Mogami H. A frameless, armless navigational system for computer-assisted neurosurgery. J Neurosurg 1991;74:845–849.
21. Kaus M, Steinmeier R, Sporer T, Ganslandt O, Fahlbusch R. Technical accuracy of a neuronavigation system measured with a high-precision mechanical micromanipulator. Neurosurgery 1997;41:1431–1436.

22. Kirsch S, Schilling C, Seiler PG. Miniaturized five degree-of-freedom magnetic tracker. In: Lemke HU, Vannier MW, Inamura K, Farman AG, editors: Computer Aided Radiology and Surgery: Proceedings of the 12th International Symposium and Exhibition (CAR'98), Tokyo, June 1998. Amsterdam: Elsevier; 1998. p 928.
23. Li Q, Zamorano L, Jiang Z, Vinas F, Diaz F. The application accuracy of the frameless implantable marker system and analysis of related affecting factors. In: Wells WM, Colchester A, Delp S, editors: Proceedings of First International Conference on Medical Image Computing and Computer Assisted Interventions (MICCAI'98), Cambridge, MA, October 1998. Lecture Notes in Computer Science 1496. Berlin, Heidelberg, New York: Springer-Verlag; 1998. p 253–260.
24. Li Q, Zamorano L, Jiang Z, Gong JX, Pandya A, Perez R, Diaz F. Effect of optical digitizer selection on the application accuracy of a surgical localization system - a quantitative comparison between the OPTOTRAK and FlashPoint tracking systems. Comp Aid Surg 1999;4:314–321.
25. Liener UC, Reinhart C, Kinzl L, Gebhard F. A new approach to computer guidance in orthopedic surgery using real time volume rendering. J Med Syst 1999; 23:35–40.
26. Maciunas RJ, Fitzpatrick JM, Galloway RL, Allen GS. Beyond stereotaxy: Extreme levels of application accuracy are provided by implantable fiducial markers for interactive image-guided neurosurgery. In: Maciunas RJ, editor: Interactive Image-Guided Surgery. Park Ridge, IL: AANS Publications Committee; 1993. p 259–270.
27. Meskers CG, Fraterman H, van der Helm FC, Vermeulen HM, Rozing PM. Calibration of the "Flock of Birds" electromagnetic tracking device and its application in shoulder motion studies. J Biomech 1999; 32:629–633.
28. Milne AD, Chess DG, Johnson JA, King GJ. Accuracy of an electromagnetic tracking device: A study of the optimal range and metal interference. J Biomech 1996;29:791–793.
29. Mulder AGE. Human Movement Tracking Technology – Technical Report. Burnaby, SC: NSERC Hand Centered Studies of Human Movement Project, Simon Fraser University; 1994.
30. Nomura T, Kobayashi E, Masamuna K, Sakuma I, Dohi T, Iseki H, Takakura K. Development of an active wireless optical marker system for optical tracking system in computer aided surgery. In: Lemke HU, Vannier MW, Inamura K, Farman AG, editors: Computer Aided Radiology and Surgery: Proceedings of the 13th International Congress and Exhibition (CARS'99), Paris, June 1999. Amsterdam: Elsevier; 1999 p 813–817.
31. Rohling R, Munger P, Hollerbach JM, Peter T. Comparison of relative accuracy between a mechanical and an optical position tracker for image-guided neurosurgery. J Image Guid Surg 1995;1:30–34.
32. Ryan MJ, Erickson RK, Levin DN, Pelizzari CA, Macdonald RL, Dohrmann GJ. Frameless stereotaxy with real-time tracking of patient head movement and retrospective patient-image registration. J Neurosurg 1996;85:287–292.
33. Sasama T, Nakahodo K, Ohzono K, Sato Y, Yoden S, Ochi T, Sugano N, Nishii T, Tamura S. Accuracy evaluation in computer assisted hip surgery. In: Lemke HU, Vannier MW, Inamura K, Farman AG, editors: Computer Aided Radiology and Surgery: Proceedings of the 13th International Congress and Exhibition (CARS'99), Paris, June 1999. Amsterdam: Elsevier; 1999. p 772–776.
34. Smith KR, Frank KJ, Bucholz RD. The NeuroStation: A highly accurate, minimally invasive solution to frameless stereotactic neurosurgery. Comput Med Imaging Graph 1994;18:247–256.
35. Trobaugh JW, Richard WD, Smith KR, Bucholz RD. Frameless stereotactic ultrasonography: Method and applications. Comput Med Imaging Graph 1994;18: 235–246.
36. Watanabe E, Watanabe T, Manaka S, et al. Three-dimensional digitizer (neuronavigator): New equipment for computed tomography-guided stereotaxic surgery. Surg Neurol 1987;27:543–547.
37. Zylka W, Sabczynski J. Effect of localization devices and registration methods on the accuracy of stereotactic frame systems predicted by the Gaussian approach. Comp Aid Surg 1999;4:77–86.